Journal of Applied Polymer Science

Study of Nanoscale Structural Changes in Isolated Bamboo Constituents Using Multiscale Instrumental Analyses

Masakazu Nishida, Tomoko Tanaka, Tsunehisa Miki, Ichinori Shigematsu, Kozo Kanayama, Wataru Kanematsu

National Institute of Advanced Industrial Science and Technology (AIST), 2266-98 Shimoshidami, Moriyama-ku, Nagoya 463-8560, Japan

Correspondence to: M. Nishida (E-mail: m-nishida@aist.go.jp)

ABSTRACT: To reveal morphological changes in bamboo constituents induced by delignification and hemicelluloses removal processes, changes in chemical composition and dynamics were examined at molecular- to nano-scales, using scanning electron microscopy images, attenuated total reflection infrared spectra, solid state nuclear magnetic resonance spectra, and relaxation time analysis at multiple hierarchical levels. Boiling removed spherical particles from the parenchymal cells of bamboo, leaving the cells containing water that had infiltrated into the nanostructure composed of carbohydrates and lignin. Treatment of the boiled bamboo with $NaClO_2$ solution removed most of lignin, leaving hemicellulose chains that made the parenchymal cells stretch. In contrast, treatment of the boiled bamboo with NaOH solution removed both hemicellulose and lignin, with the result that parenchymal cells shrank in the cross-section direction. Furthermore, treatment of the delignified bamboo with NaOH solution demolished the parenchymal cells due to complete removal of hemicellulose and lignin. A nanostructural model proposed on the basis of molecular- to nano-scale analyses was consistent with the changes of vascular bundles and parenchymal cells. © 2013 Wiley Periodicals, Inc. J. Appl. Polym. Sci. **2014**, *131*, 40243.

KEYWORDS: properties and characterization; morphology; spectroscopy; microscopy; biopolymers; renewable polymers

Received 20 September 2013; accepted 1 December 2013

DOI: 10.1002/app.40243

INTRODUCTION

Vegetation materials are the most easily available bioresources and their utilization and application have actively expanded into not only the fabrication of materials themselves but also into manufacturing composite materials with other components.[1,2] Among vegetation materials, bamboo is commonly used because it is easily obtained and processed; thus, it has been used in handicrafts since ancient times. In addition to this classical fabrication of bamboo products, recent developments in wood science have focused on utilizing bamboo as raw materials for various industries. Bamboo pulp is a well-known raw material and has been modified with chemicals such as acetic acid[3] and formic acid.[4] Appropriate chemical modification of bamboo can also provide each of its constituents: polysaccharide,[5] cellulose,[6] hemicellulose,[7] and lignin.[8]

A number of interesting applications of bamboo pulps and bamboo fibers used as a base component for manufacturing composite materials have been published. Natural rubber composites were prepared from bamboo cellulose nanofibers and nanowhiskers and their diffusion, sorption, and permeation properties were examined.[9] Bamboo charcoal/polyoxometalate nanocomposites were prepared as biological protective materials.[10] Bamboo fibers have also featured as constituents of composite materials with a biodegradable unit; for instance, bamboo fibers improved the mechanical properties of poly(lactic acid).[11] Hybrid biocomposites consisting of poly(lactic acid)/bamboo fiber/talc were prepared and their heat distortion were examined, focusing on crystallinity.[12] Furthermore, molding materials based on bamboo composites were produced, such as plastic composite panels[13] and wood-ceramics made from epoxy resin.[14] To better advance these recent developments in bamboo composites, convenient analytical methods for bamboo are urgently required.

Solid state nuclear magnetic resonance (NMR) is a useful analytical method in a wide range of industrial fields because preparation and recovery of samples is easy. Thanks to advances in electronic devices and measurement technologies, solid state NMR has expanded its range of application to wood products[15] and food science.[16] Since the 1990s, bamboo has become a new subject for solid state NMR studies: for changes of chemical composition with growth of immature bamboo[17] and internodal

growth of bamboo[18] using ^{13}C cross polarization and magic angle spinning (CP-MAS) NMR. The recent use of solid state NMR heralds a new molecular level approach to the use of bamboo in materials manufacture. For example, structural changes of bamboo after hydrolysis with formic acid were studied with ^{13}C CP-MAS NMR and X-ray diffraction.[4] In a study of bioethanol production from bamboo, ^{13}C CP-MAS NMR gave useful information on the cellulose rich fraction.[19] To study crystalline allomorphs, cellulose acetate derived from bamboo was analyzed by ^{13}C CP-MAS NMR together with Fourier transfer infrared (FTIR) and X-ray diffraction.[20] Solid state ^{13}C CP-MAS NMR also revealed differences in the morphological characteristics of bamboo fibers from other natural cellulose fibers.[21]

On the other hand, we have been studying not only the functionalization of bamboo for manufacturing applications but also new analytical methods for bamboo used as a starting material for new functional products. For example, we reported the relationship between thermal-softening properties and deformation, appearing after heating and cooling of load-carrying bamboo.[22] Meanwhile, as a new analytical method for biomass polymers, we have studied solid state NMR analysis of poly(lactic acid) as follows. The correlation between polymer composition and mechanical properties was analyzed using ^{13}C MAS NMR spectra and magnetic relaxation times.[23] Additionally, as examples of composites of biomass polymer and inorganic fillers, poly (lactic acid)/clay nanocomposites were analyzed using ^{13}C CP-MAS NMR together with X-ray diffraction, scanning electron microscopy (SEM), and TEM.[24] Based on our knowledge of the chemical composition and properties of biomass polymers provided by solid-state NMR, we have been studying improvements in instrumental analyses for bamboo manufacturing processes. Here, we focus on several processes that separate the components of bamboo, using multiscale instrumental analyses using solid state NMR and attenuated total reflection infrared (ATR-IR) as molecular- to nano-scale spectroscopic analyses as well as SEM for micron-scale morphological analysis.

EXPERIMENTAL

Materials

Microcrystalline cellulose powder (average particle size 20 μm) purchased from Aldrich was used a standard material. Standard high-purity cellulose fibers (average particle size 50 μm) were purchased from Scientific Polymer Products. Xylan from Oat spelt was purchased from Nacalai Tesque. Xylan from beechwood was purchased from Sigma Life Science. Lignin (Alkaline) and Lignin (Dealkaline) were purchased from Tokyo Chemical Industries. The completely lignified bamboo chosen in this article was Moso bamboo (*Phyllostachys pubescens* Mazel) that was more than 3 years old from the Aichi prefecture of Japan. Fibers that were about 1-mm thick from the same internodes were used as bamboo specimens. A pretreatment to remove components consisted of boiling in water for 8 h. Afterward, delignification was performed with a 4% $NaClO_2$ solution according to the Klaudiz method.[25] Removal of hemicellulose was performed by the addition of dilute NaOH solution followed by heating at 120°C.[25] Specimens that had been both delignified and had hemicellulose removed were also prepared by a reaction of the delignified bamboo with dilute NaOH solution.

Scanning Electron Microscopy

SEM images were recorded with a JEOL JSM-5600ED (Tokyo, Japan) at an acceleration voltage of 3–20 kV. The specimen was sliced along the longitudinal section and was coated by gold-sputtering in a vacuum using an ULVAC QUICK COATER VPS-020 (Chichibu, Japan). Low magnification SEM images (100–250×) were obtained from specimens cut by dissection scissors and high magnification SEM images (1000–3000×) were taken from specimens whose surfaces were first smoothed by a microtome and then fixed with an adhesive.

Infrared Spectroscopy

FTIR spectra were measured on a Thermo Scientific Nicolet 6700 FTIR spectrometer (Waltham, MA) with 4 cm^{-1} resolution and 32 scans in the range 550–4000 cm^{-1}. The ATR method was applied for the data collection using a Thermo Scientific SMART iTR single reflection diamond ATR attachment (Waltham, MA) at ambient temperature.

NMR Measurements

The solid state NMR spectra were measured on a Varian 400 NMR system spectrometer (Palo Alto, CA) over a temperature range of 22°C to 28°C. The ^{1}H MAS NMR spectra (399.86 MHz) were measured with a Varian 1.6 mm FastMAS probe with a 36 kHz sample spinning (0.2 sec acquisition period; 1.2 μsec $\pi/2$ pulse for the ^{1}H nuclei; 3.0 sec recycle delay). The ^{13}C MAS NMR spectra (100.56 MHz) were measured with a Varian 4 mm double-resonance T3 solid probe with a 15 kHz sample spinning and were collected with 40 msec acquisition period and an 86 kHz ^{1}H decoupling radio frequency with a small phase incremental alteration decoupling pulse sequence.[26] The CP-MAS NMR spectra were measured with a 5.0 sec recycle delay using a ramped-amplitude pulse sequence[27] with a 2 msec contact time and a 2.6 μsec $\pi/2$ pulse for the ^{1}H nuclei. The amplitude of the ^{1}H nuclei was ramped down linearly from 92.6% of its final value during the cross polarization contact time. Single ^{13}C pulse measurements used a 4.8 μsec $\pi/2$ pulse for the ^{13}C nuclei and are represented in this article by DD-MAS (dipolar decoupling and magic angle spinning) NMR with a 60 sec recycle delay. Pulse saturation transfer and magic angle spinning (PST-MAS) NMR was measured with a 4.8 μsec $\pi/2$ pulse for the ^{13}C nuclei with a 5 sec recycle delay after saturation of ^{1}H nuclei with five consecutive 2.6 μsec pulses and a 27.5 μsec delay.

Nuclear Magnetic Relaxation Time Analysis

The ^{1}H spin-lattice relaxation time in the laboratory frame (T_1H) was indirectly measured via the detection of the ^{13}C resonance and enhanced by the cross-polarization applied after a π pulse to the ^{1}H nuclei with the inversion recovery method. The ^{13}C spin-lattice relaxation time in the laboratory frame (T_1C) was measured with the conventional Torchia's pulse sequence.[28] The relaxation time analyses were performed with the same solid state probe with the same contact time and acquisition period used for the ^{13}C CP-MAS NMR spectrum.

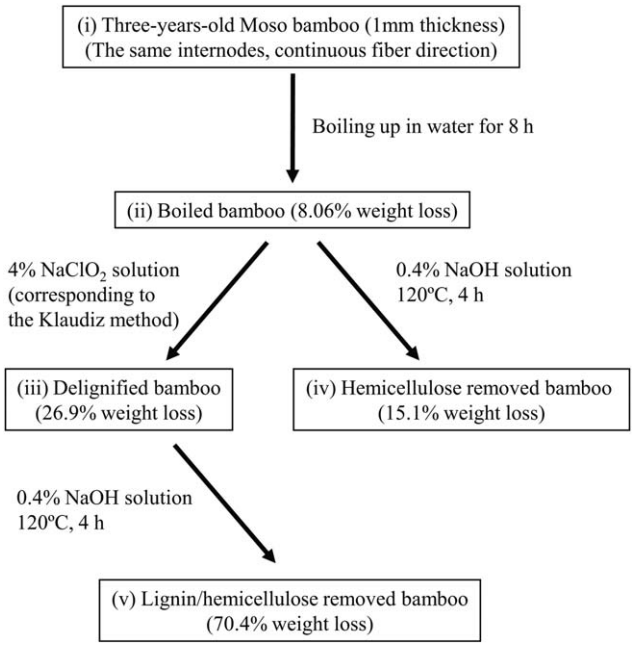

Figure 1. Scheme for chemical treatments of bamboo.

RESULTS AND DISCUSSION

Morphological Analysis of Bamboo due to Delignification and Hemicellulose Removal Processes

Figure 1 gives an outline of the chemical treatments used in delignification and hemicellulose removal processes. At first, a bamboo specimen (i) was boiled in water to remove water-soluble low molecular weight inclusions. Although an 8.06% weight loss occurred for the boiled specimen (ii), little changes in the specimen shape were observable by the naked eye during the boiling process. Next, this boiled specimen was taken and used the delignification and hemicellulose removal processes: treatment with a 4% $NaClO_2$ solution decolorized the bamboo specimen with a 26.9% weight loss in the delignification process (iii), while treatment with a 0.4% NaOH solution led to a twisted bamboo specimen with a 15.1% weight loss in the hemicellulose removal process (iv). The decolorized specimen delignified by a $NaClO_2$ solution was further treated with 0.4% NaOH solution to produce white small pieces with a 70.4% weight loss (v).

Morphological changes due to the delignification and hemicellulose removal processes were investigated in more detail by SEM. At first, we examined changes in cross-sectional images of bamboos during the chemical modifications, as shown in Figure 2. At low magnification, the cross-section shape of the untreated bamboo featured several vascular bundles dispersed in parenchymal cells [Figure 2(i)]. A considerable number of spherical particles could be observed in the parenchymal cells of the untreated bamboo at high magnification [Figure 2(i′)]. While the low magnification SEM image of the boiled specimens indicated that the bore sizes of parenchymal cells were somewhat increased [Figure 2(ii)] compared with untreated ones, the high magnification image showed that the spherical particles in the parenchymal cell had been completely removed [Figure 2(ii′)]. Although little changes were apparent in the low magnification SEM image of the delignified specimen [Figure 2(iii)] compared with the boiled one, the cross section of the parenchymal cell was not flat, but showed a stretched shape at high magnification [Figure 2(iii′)]. On the other hand, the hemicellulose removal process caused more significant changes in the parenchymal cell. The low magnification SEM image [Figure 2(iv)] showed that the volume of the parenchymal cell was reduced and the proportion of the vascular bundle in the cross-

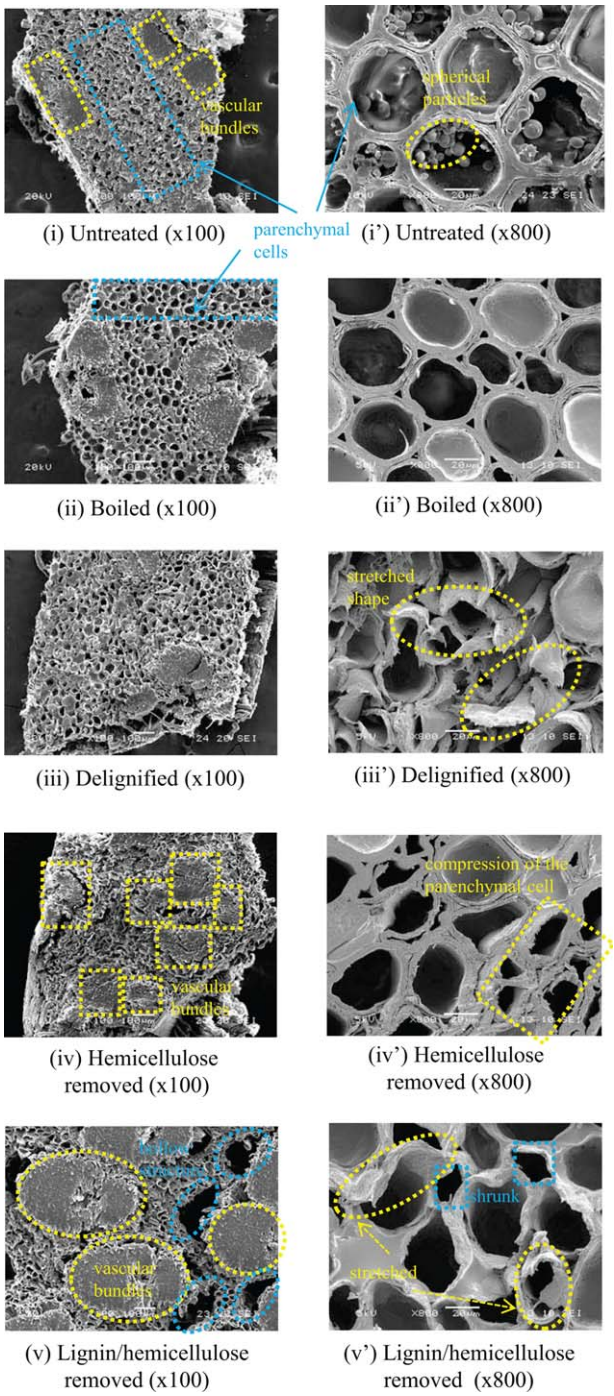

Figure 2. Scanning electron micrographs of bamboo cross sections of denatured bamboos. [Color figure can be viewed in the online issue, which is available at wileyonlinelibrary.com.]

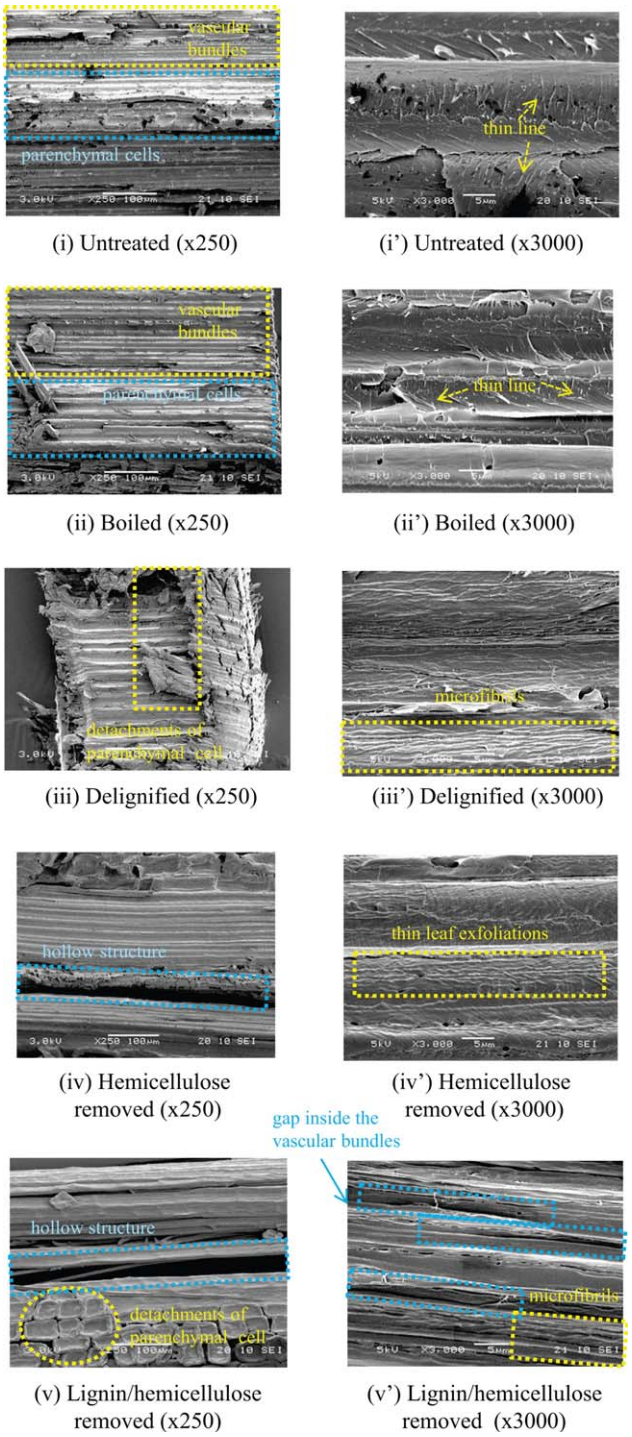

Figure 3. Scanning electron micrographs of lengthwise bamboo sections of denatured bamboos. [Color figure can be viewed in the online issue, which is available at wileyonlinelibrary.com.]

section shape increased. This volume reduction of the parenchymal cell was confirmed by the compression of the parenchymal cell in the high magnification SEM image [Figure 2(iv′)]. Furthermore, many parts of parenchymal cells were lost and showed a hollow structure in the lignin/hemicellulose removed specimen [Figure 2(v)] and the remaining parenchymal cells were both stretched and shrunken [Figure 2(v′)].

Next, we investigated changes in the lengthwise sections of bamboos after the chemical modifications, as shown in Figure 3. In both low and high magnification SEM images, there were no obvious differences between untreated [Figure 3(i,i′)] and boiled [Figure 3(ii,ii′)] specimens: one can see vascular bundles as narrow parallel lines and parenchymal cells as relatively broad features in low magnification images, and thin lines appear over the vascular bundle in the high magnification images. In the delignified specimens, the ends of lengthwise-section and some parenchymal cells appeared deformed in the low magnification SEM image [Figure 3(iii)]. Interestingly, microfibrils were present over the vascular bundles of the delignified specimens in the high magnification SEM image [Figure 3(iii′)]. Meanwhile, in the specimen which had undergone hemicellulose removal, some parenchymal cells detached in fragments, resulting in the formation of gaps between vascular bundles [Figure 3(iv)]. Although thin leafs exfoliated from the surface of the vascular bundle of the hemicellulose-removed specimen, the existence of microfibrils was obscured [Figure 3(iv′)]. The fragmentation of the parenchymal cell and the gaps between the vascular bundles were more conspicuous in the lignin/hemicellulose removal specimen [Figure 3(v)]: the parenchymal cells became detached flat sheets and the vascular bundles were torn to several thin bundles. Although microfibrils over the vascular bundle remained to a certain degree, gaps inside the vascular bundles were also observed at high magnification [Figure 3(v′)].

ATR-IR Spectra Changes of Bamboo due to Delignification and Hemicellulose Removal Processes

In order to investigate the morphological changes in relation to the chemical nature of the bamboo components, ATR-IR spectra were recorded for various extents of removal in each removal process. Vibrational assignment of characteristic bands for bamboo was based on previous literature.[29,30] Figure 4(A) shows changes in the ATR-IR spectra of bamboo produced by the boiling and delignification processes, with a magnified view between 1000 and 1800 cm^{-1} shown in Figure 4(B). Significant bands unchanged by the removal processes appeared at 3100–3500, 2800–2950, and 980–1080 cm^{-1} [Figure 4(A)], which were assigned as O—H stretch, C—H stretch, and C—O bond vibrations, respectively. Spectral changes due to the boiling process [Figure 4(B), line (ii)] were limited to very small changes in peak shapes, although the SEM image indicated the removal of spherical particles from the parenchymal cell. In contrast, the delignification process significantly influenced the ATR-IR spectra, especially in the range from 1800 to 1100 cm^{-1}. Even for a low degree of delignification, a rapid decrease appeared in the 1450–1470 and 1490–1530 cm^{-1} peaks [Figure 4(B), line (iii)], assigned as asymmetric C—H bending from OCH_3 and aromatic skeletal vibrations, respectively. The overlapped peaks of aromatic skeletal vibration and C=O stretch appeared at 1570–1620 cm^{-1}, and they gradually changed during the delignification process. The vibration at 1700–1750 cm^{-1}, which was assigned the C=O stretch and C=O valence vibration bands, also gradually reduced in the course of the delignification process. In the case of the most delignified specimen [Figure 4(B), line (v)], the peak due to the C=O bond [arrow (1)] still remained, although asymmetric C—H bending bands from

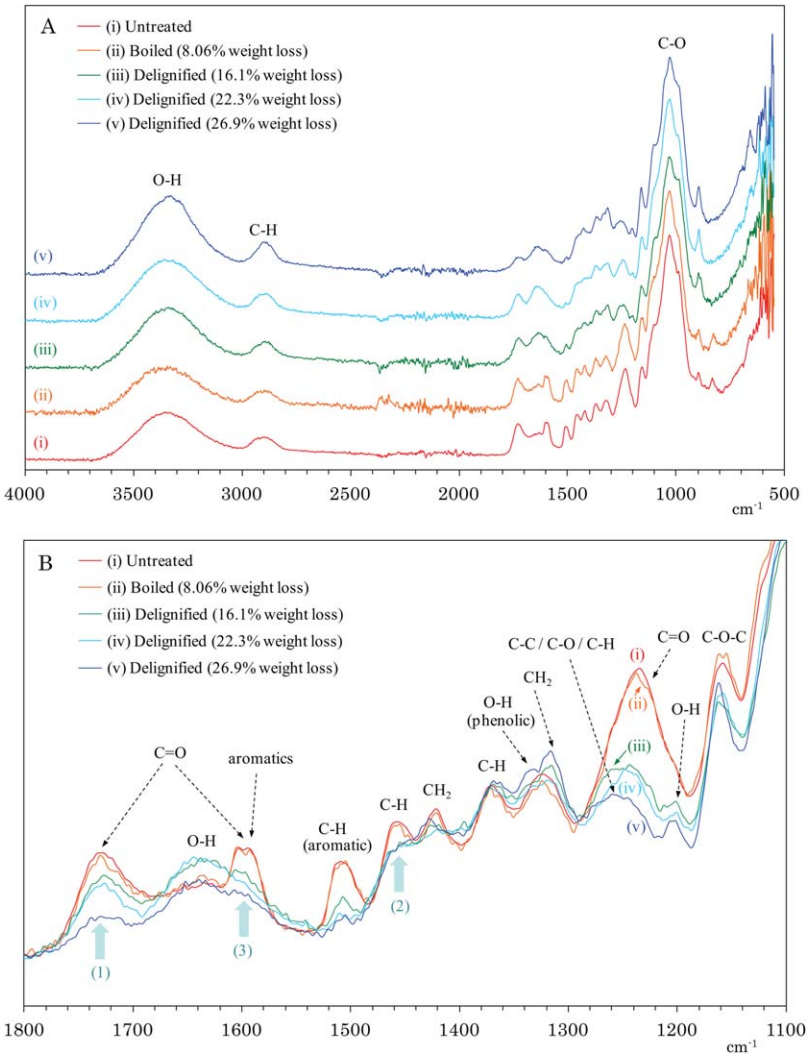

Figure 4. ATR-IR spectra changes of bamboo in boiling and delignification processes (A: in full range; B: in the range from 1800 to 1100 cm^{-1}). [Color figure can be viewed in the online issue, which is available at wileyonlinelibrary.com.]

OCH_3 (2) and aromatic skeletal vibrations (3) had almost disappeared, as indicated by upward pointing arrows. The spectral changes noted above indicated that the aromatic ring containing OCH_3 was removed at an early stage of the delignification process, and then the remaining C═O group started to be removed. Namely, delignification first occurred at the ester bond between lignin and hemicellulose, and then monolignol units were removed by the decomposition of the three-dimensional lignin network. The C═O group associated with the hemicellulose unit was still in place after the delignification process.

Figure 5(A) shows changes in the ATR-IR spectra of bamboo produced by the hemicellulose removal and lignin/hemicelluloses removal processes, with a magnified view between 1000 and 1800 cm^{-1} shown in Figure 5(B). For the specimen with a low degree of hemicellulose removal [Figure 5(B), line (ii)], a rapid decrease in the C═O stretch peak at 1700–1750 cm^{-1} was observed. The hemicellulose removal process led to gradual changes in the 1450–1470 cm^{-1} (C—H deformation), 1410–1430 cm^{-1} (CH_2 scissoring), 1350–1390 cm^{-1} (C—H deformation), and 1300–1350 cm^{-1} (O—H, CH_2 rocking) bands, which were all assigned to sugar chains. Interestingly, the characteristic bands of lignin [the asymmetric C—H bending from OCH_3: 1450–1470 cm^{-1} [arrow (1)]; the aromatic skeletal vibration: 1490–1530 (2); and 1570–1620 cm^{-1} (3)] also decreased with the degree of hemicellulose removal, as indicated by upward pointing arrows. The relative tendency of bands to reduce during hemicellulose removal indicated that the first attack occurred at the ester bond to remove hemicellulose together with the C═O group and that lignin decomposition accompanied higher degrees of hemicellulose removal [Figure 5(B), line (iii)].

Relatively large peaks in the 1190–1300 cm^{-1} region were produced by the overlap of several peaks originating from cellulose, hemicellulose, and lignin. These vibrations also changed in characteristic ways in the removal processes as follows. In the delignification process, the overlapped peaks changed into a bimodal pattern at 1190–1220 and 1230–1290 cm^{-1} [Figure 4(B), lines (iii–v)], which were assigned to O—H in-plane bending and C—H bending in carbohydrates, respectively. In the hemicellulose

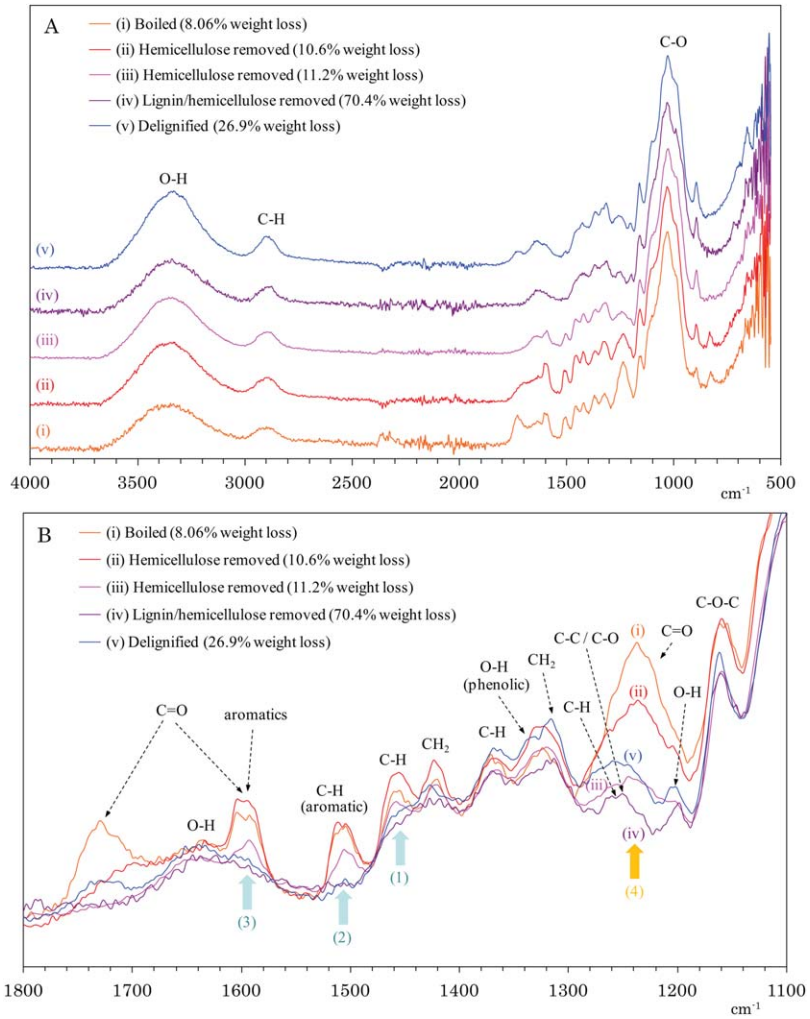

Figure 5. ATR-IR spectra changes of bamboo in hemicellulose removal and lignin/hemicellulose removal processes (A: in full range; B: in the range from 1800 to 1100 cm^{-1}). [Color figure can be viewed in the online issue, which is available at wileyonlinelibrary.com.]

removal process, C—C, C—O, and C═O vibrations decreased at the same time; thus, the intensity in the 1190–1300 cm^{-1} region [arrow (4)] reduced as a single peak [Figure 5(B), lines (ii) and (iii)]. In the lignin/hemicellulose removal process [Figure 5(B), line (iv)], the intensity in the 1190–1300 cm^{-1} region substantially reduced to show a clearer bimodal vibration pattern because the C═O stretch vibration completely disappeared and the intensity of the O—H in-plane bending and C—H bending vibrations in hemicellulose remained at a low level. In the ATR-IR spectra of the lignin/hemicellulose-removed specimen, not only the aromatic vibrations of lignin but also the C═O vibrations completely disappeared to significantly reduce the overall peak intensity of the spectra.

^{1}H MAS NMR and ^{13}C CP-MAS NMR of Untreated Bamboo and Standard Materials

As described earlier, SEM is a powerful tool to examine the morphology over a region larger than 1 μm, and ATR-IR is a suitable method to determine chemical functionalities in the vicinity of the surface. Considering that the ATR-IR spectra could not detect the removal of spherical particles seen in the SEM image, the ATR-IR method was not suitable for examining the chemical composition and bulk structures of the bamboo. Hence, we applied the solid state NMR method to further analyze chemical removal processes for bamboo focusing on ^{1}H and ^{13}C nuclei with several pulse sequences. To help in making signal assignments for bamboo, spectra of the following standard materials were also measured: cellulose fibers (average particle size: 50 μm) and cellulose powder (average particle size: 20 μm); xylan of oat spelt and xylan of beech wood as a typical hemicellulose sample; alkaline lignin and dealkaline lignin.

Figure 6(A) shows ^{1}H MAS NMR spectra of bamboo specimens resulting from the chemical treatment, compared with those of the standard materials taken as components of bamboo. Peaks appearing around 5 ppm were assigned as free water and became a standard of mobility in the components that constituted bamboo in its natural form. That is, the free water in cellulose and xylan from oat spelt showed a sharp peak shape [Figure 6(A), lines (vi–viii)] and had relatively high mobility, while the free water in xylan from beech wood and lignin showed a broad peak shape [Figure 6(A), lines (ix–xi)] and had lower mobility. Because of the presence of broad free water peaks, the mobility of the free water in bamboos was lower

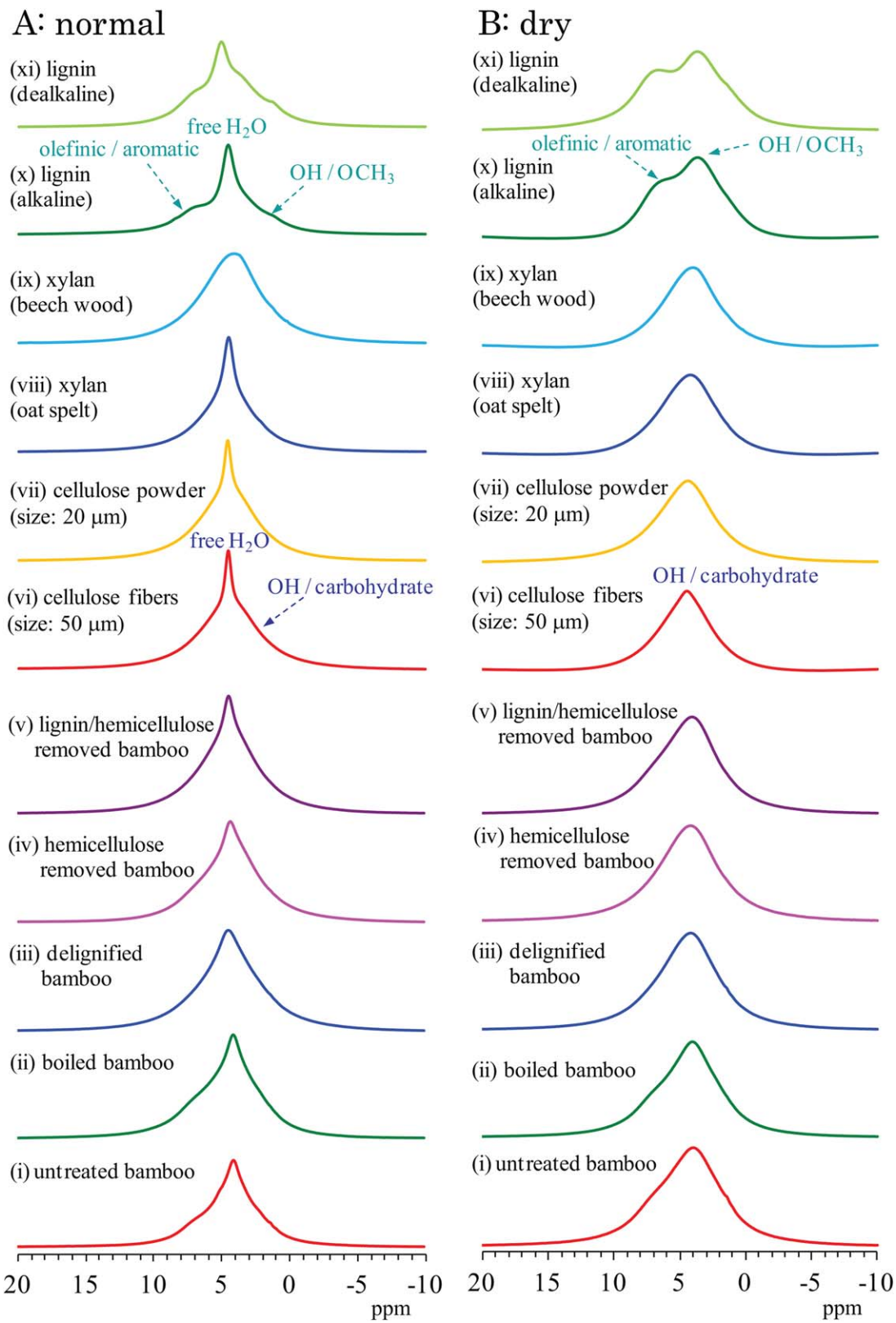

Figure 6. ^{1}H MAS NMR spectra of denatured bamboos and standard materials (A: in a normal condition; B: in a dry condition). [Color figure can be viewed in the online issue, which is available at wileyonlinelibrary.com.]

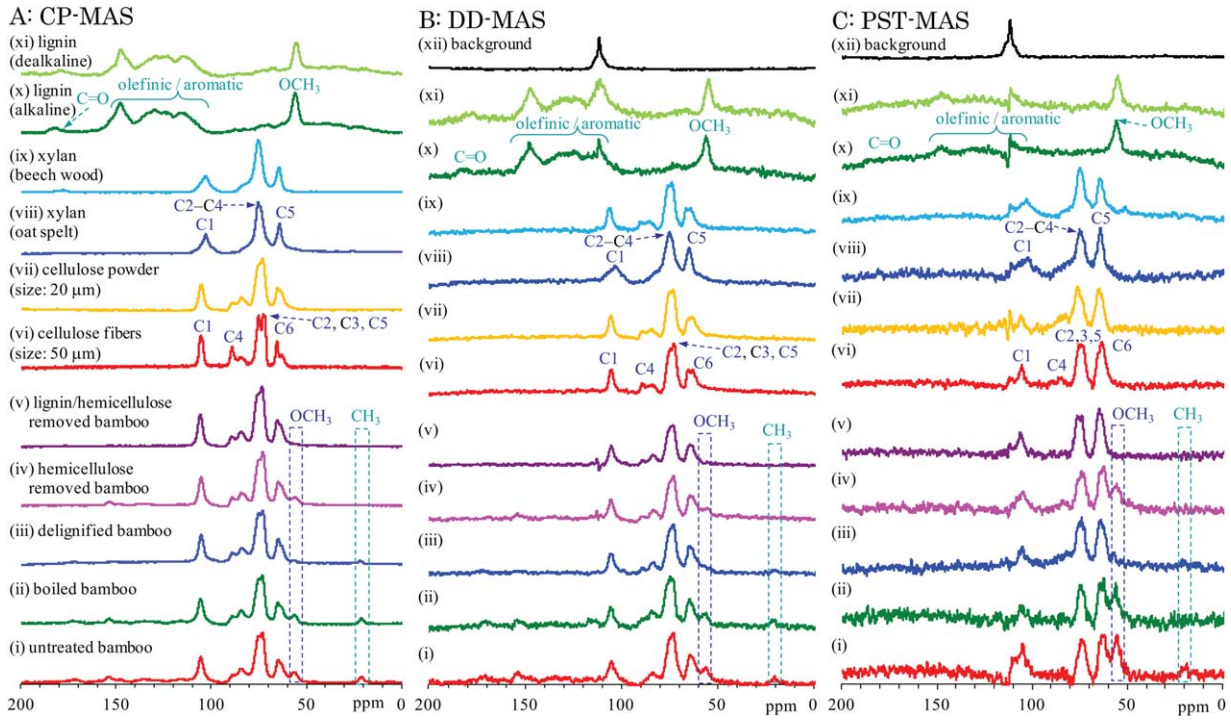

Figure 7. ^{13}C MAS NMR spectra of denatured bamboos and standard materials (A: CP-MAS pulse sequence; B: DD-MAS pulse sequence with background correction; C: PST-MAS pulse sequence with background correction). [Color figure can be viewed in the online issue, which is available at wileyonlinelibrary.com.]

regardless of the chemical modifications, as shown in Figure 6(A), lines (i–v). The free water was easily removed by a nitrogen gas purge at 80°C. Figure 6(B) shows ^{1}H MAS NMR spectra of the standard materials and the bamboo specimens in a dry condition. Cellulose and xylan showed very broad peaks, which consisted of overlapped proton signals of hydrocarbon and hydroxyl groups [Figure 6(B), lines (vi–ix)]. Lignin had a broad biphasic peak consisting of aromatic protons in addition to the signals of hydrocarbon and hydroxyl groups [Figure 6(B), lines (x–xi)]. In all the bamboo specimens [Figure 6(B), lines (i–v)], the aromatic proton signal was very small, even in material that had not been delignified.

As shown above, chemical modification of bamboos produced only small changes in the ^{1}H MAS NMR spectra. Accordingly, changes in ^{13}C CP-MAS NMR spectra were examined for each removal process in order to separate the signal of each component. Assignments of ^{13}C CP-MAS NMR signals for the components can be found in a previous publication.[31] Figure 7(A) shows ^{13}C CP-MAS NMR spectra of the bamboo specimens [Figure 7(A), lines (i–v)], compared with the spectra of the standard materials [Figure 7(A), lines (vi–xi)] consisting of bamboo. The ^{13}C CP-MAS NMR spectrum of the untreated bamboo [Figure 7(A), line (i)] was assigned to each component as follows. Major ^{13}C peaks in the spectra of the untreated bamboo originated from carbohydrates: amorphous C6 carbon atoms in carbohydrates (63 ppm) and crystalline C6 carbon atoms in carbohydrates (66 ppm), C2, C3, and C5 carbon atoms in carbohydrates (73 ppm and 76 ppm), amorphous C4 carbon atoms in carbohydrates (84 ppm), crystalline C4 carbon atoms in carbohydrates (89 ppm), and C1 carbon atoms in carbohydrates (105 ppm). Signals of sugars in hemicellulose overlapped (C5: 64 ppm; C2–4: 75 ppm; C1: 102 ppm) with those of carbohydrates in cellulose. A higher field peak (22 ppm) in the untreated bamboo could not be observed in any standard materials measured. In previous papers,[31,32] however, this peak was assigned as CH_3 in acetyl groups of hemicellulose according to measurements on oak wood and pine wood. Signals derived from lignin appeared as small broad peaks: 55 ppm (OCH_3), 110–160 ppm (olefinic and aromatic carbon atoms), and 166–180 ppm (carbonyl groups). According to the spectral assignments of lignin [Figure 7(A), lines (x and xi)], the olefinic and aromatic carbon atoms belonged to three regions as follows: 110–124 ppm (unsubstituted olefinic or aromatic carbon atoms), 124–142 ppm (quaternary olefinic or aromatic carbon atoms), 142–162 ppm (olefinic or aromatic carbon atoms with OH or OR substituents).

^{13}C DD-MAS NMR and ^{13}C PST-MAS NMR of Untreated Bamboo and Standard Materials

The ^{13}C CP-MAS NMR method uses cross polarization from ^{1}H nuclei to ^{13}C nuclei; hence, the peak intensity is low in the case of a quaternary carbon atom having no protons, as well as carbon atoms in molecular with high mobility. It was possible to observe the less sensitive carbon atoms in ^{13}C CP-MAS NMR using a 60 sec recycle time between acquisition periods. A background signal also appeared at 113 ppm; thus, we presented ^{13}C DD-MAS NMR spectra after background correction using the spectrum of the empty rotor. Figure 7(B) shows ^{13}C DD-MAS NMR spectra of the bamboo specimens referred to the spectra

of the standard bamboo materials. Compared with CP-MAS spectra, the DD-MAS NMR spectrum of cellulose fibers [Figure 7(B), line (vi)], the signal of the crystalline carbon atoms (66 ppm and 89 ppm) reduced and changed to the peak shape of carbohydrates, although the C4 carbon peaks (84 ppm and 88 ppm) of carbohydrates significantly increased in the DD-MAS NMR spectrum of xylan (beech wood), as shown in Figure 7(B), line (ix). The DD-MAS NMR spectra of cellulose powder and xylan oat spelt [Figure 7(B), lines (vii and viii)] were quite similar to their CP-MAS NMR spectra [Figure 7(A), lines (vii and viii)]. In the case of lignin [Figure 7(B), lines (x and xi)], the signals of unsubstituted olefinic or aromatic carbon atoms (110–124 ppm) in the DD-MAS seemed to increase compared with those in the CP-MAS; however, because the background signal appeared in the same region, the alternation of these signals was unclear. According to the assignments of the standard materials mentioned above, the signals of the olefinic or aromatic carbon atoms with OH or OR substituents (142–162 ppm) increased in the ^{13}C DD-MAS NMR spectrum of the untreated bamboo [Figure 7(B), line (i)].

In high mobility molecules, the signal intensity reduced in the CP-MAS NMR spectra due to spin diffusion via ^{1}H nuclei. Thus, in order to exclude the spin diffusion of the high mobility molecules, ^{13}C PST-MAS NMR spectra measured using a single ^{13}C pulse after saturation of the ^{1}H nuclei are shown in Figure 7(C). Because the background signal also appeared in the same region as those of unsubstituted olefinic or aromatic carbon atoms in lignin (110–124 ppm) [Figure 7(C), line (xii)], we present the spectra in Figure 7(C) as differential spectra to remove the signal from the empty rotor. In the ^{13}C PST-MAS NMR spectra, the signal intensities of high mobility molecules increased compared with those in the CP-MAS, such as the C6 carbon atom (63 ppm) in cellulose, the C5 carbon atom (64 ppm) in xylan, and OCH_3 (55 ppm) in lignin. In contrast, higher field signals in lignin decreased and weak peaks of olefinic or aromatic carbon atoms with OH or OR substituents (142–162 ppm) remained. Like the standard materials, the ^{13}C PST-MAS NMR spectrum of untreated bamboo [Figure 7(C), line (i)] showed a different peak pattern from the ^{13}C CP-MAS NMR [Figure 7(A), line (i)]. The major signals were OCH_3 in lignin (55 ppm) and two carbon atom signals in carbohydrates of cellulose and hemicellulose (64 ppm and 75 ppm), while the minor signals were CH_3 in acetyl groups (22 ppm) and C1 carbon atoms in carbohydrates (105 ppm), although the latter minor signal suffered from interference from the background peak.

Relaxation Time Analysis of Bamboo of Untreated Bamboo and Standard Materials

To investigate the molecular dynamics and environment of the denatured bamboo revealed by spin diffusion, we further analyzed the ^{1}H spin-lattice relaxation time in the laboratory frame (T_1H) and ^{13}C spin-lattice relaxation time (T_1C). Figure 8(A) shows the T_1H value of the standard materials and the untreated bamboo. The T_1H values of xylan depended on the raw material: xylan originated from oat-spelt had very long T_1H values (4.1–4.5 sec), while xylan originating from beechwood had lower T_1H values (1.0–1.1 sec). In contrast, the T_1H values of cellulose were slightly affected by the specimen shape: fibers (3.7–3.9 sec); powder (3.4–3.6 sec). Moreover, the T_1H values of lignin showed little difference due to the manufacturing method (alkaline: 0.62–0.70 sec; dealkaline: 0.56–0.67 sec), except for C═O (0.43 sec) and CH_3 of those (0.27 sec) of dealkaline lignin. Untreated bamboo mainly consists of cellulose, hemicellulose, and lignin, of which T_1H values clearly changed. That is, T_1H's of carbohydrates increased to 1.8–2.2 sec while the T_1H's of C═O and CH_3 of lignin dropped to 1.0 and 1.5 sec, respectively. This equalization of the T_1H values seems to be caused by the spin diffusion between carbohydrate and lignin.

Meanwhile, the T_1C values in Figure 9(A) were larger and more scattered compared with the T_1H values in the high field region (below 100 ppm), where the signal of carbohydrates and OCH_3 of lignin appeared. The T_1C values of carbohydrates had the following values: cellulose fibers (26–44 sec), cellulose powder (23–41 sec), xylan beechwood (15–37 sec), and xylan oat-spelt (17–35 sec). As for the T_1C values of lignin, OCH_3 had a short T_1C value (alkaline: 3.6 sec; dealkaline: 2.9 sec), although olefinic or aromatic carbon atoms had rather long T_1C value (alkaline: 16–30 sec; dealkaline: 18–24 sec). In addition, the T_1C of untreated bamboo showed long values for both carbohydrates (16–40 sec) and for the OCH_3 of lignin (2.4 sec), similar values to those of the isolated materials.

Changes in Solid State NMR Spectra and Relaxation Time T_1 in the Delignification and Hemicellulose Removal Processes

Based on the assignments of solid state NMR in sections "^{1}H MAS NMR and ^{13}C CP-MAS NMR of untreated bamboo and standard materials" and "^{13}C DD-MAS NMR and ^{13}C PST-MAS NMR of untreated bamboo and standard materials," we investigated changes at the molecular level in the delignification and hemicellulose removal processes. Figures 8(B) and 9(B) show the changes of T_1H and T_1C values in the delignification and hemicellulose removal processes, respectively. On boiling, the removal of spherical particles from the parenchymal cell was a characteristic change in the greater than 1 μm size regime [Figure 2(v′)]. This removal process could not be detected by ATR-IR spectra [Figure 4(B), line (ii)]. Although the solid state NMR spectra taken with the regular pulse sequences (^{1}H MAS, ^{13}C CP-MAS, and ^{13}C DD-MAS) were hardly changed in the boiling process, the peak intensity of OCH_3 was somewhat reduced in the ^{13}C PST-MAS NMR [Figure 7(C), line (ii)]. The changes for carbohydrate signals in the boiling process were more obvious for the T_1H values, which reduced to about 1.4 sec [Figure 8(B)]. These reductions of the T_1 values were caused by introduction of free water in the interface, and formation of hydrogen bonds between bamboo constituents. As shown in Figure 9(B), the T_1C values of carbohydrates also shortened in the boiling process, probably due to the removal of water-soluble spherical particles; the T_1C values decreased from 16–40 sec to 11–30 sec.

Although the boiling process had a limited influence on the spectroscopic data, the delignification process significantly changed both the morphology and the spectroscopic data. The major change in all the ^{13}C MAS NMR spectra [Figure 7,

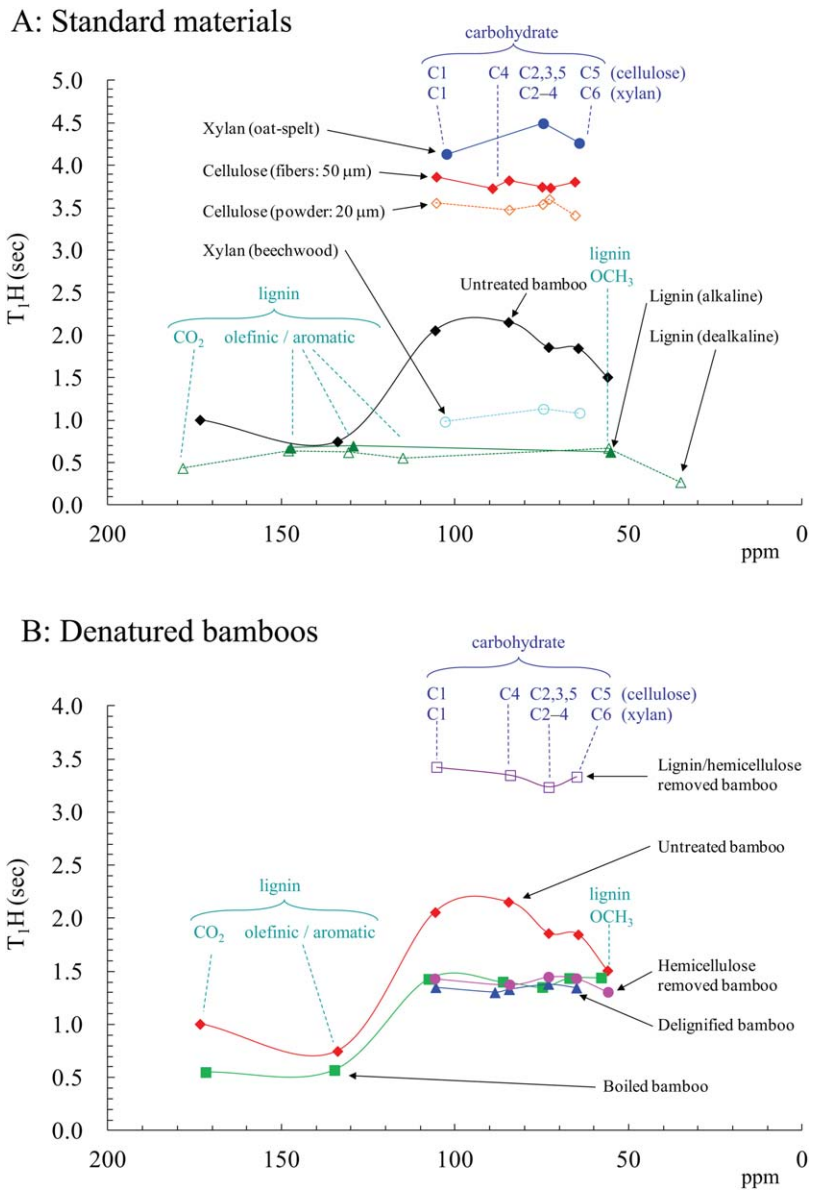

Figure 8. Changes of T_1H values (A: the standard materials; B: denatured bamboos). [Color figure can be viewed in the online issue, which is available at wileyonlinelibrary.com.]

lines (iii)] appeared for the signals of OCH_3, which decreased to a very weak intensity. With regard to the other signals originating from lignin, the C═O and olefinic or aromatic carbon atoms remained, especially in the ^{13}C DD-MAS NMR spectra; however, the latter olefinic or aromatic carbon atoms almost disappeared in the ATR-IR spectra [Figure 4(B), line (v)]. Namely, the remaining lignin units existed not in the surface, but in the bulk of the specimen. On the other hand, although changes in the carbohydrate signals were unclear in the ^{13}C MAS NMR and ATR-IR spectra, the T_1C values of carbohydrates further shortened in the delignification process (16–40 sec → 11–30 sec → 8.5–23 sec), as shown in Figure 9(B). Correlating these spectral changes with the morphological observations leads to the conclusion that the delignification process disarranged the three-dimensional network structure of lignin in the parenchymal cell, even though a part of the lignin unit remained. This disarrangement brought about the stretched shape of parenchymal cell [Figure 2(iii′)] and made the microfibrils rise over the vascular bundles [Figure 3(iii′)].

The changes produced in the ^{13}C MAS NMR by the hemicellulose removal process were less decipherable than the deliginification process because the hemicellulose signals overlapped with those of cellulose: the reduced peak intensity of hemicellulose carbohydrates modified the 70–80 ppm peak shape in the ^{13}C CP-MAS NMR of the hemicellulose-removed specimen [Figure 7(A), line (iv)]. On the other hand, the T_1C values of the hemicellulose-removed specimen (4.0–24 sec) were shortened more than those of the delignified specimen (8.5–23 sec) [Figure 9(B)]. An apparent decrease in the ^{13}C CP-MAS NMR intensity occurred not for the carbohydrate signals, but rather for those from substituents connected with hemicellulose: the signals of CH_3 and C═O evanesced after the

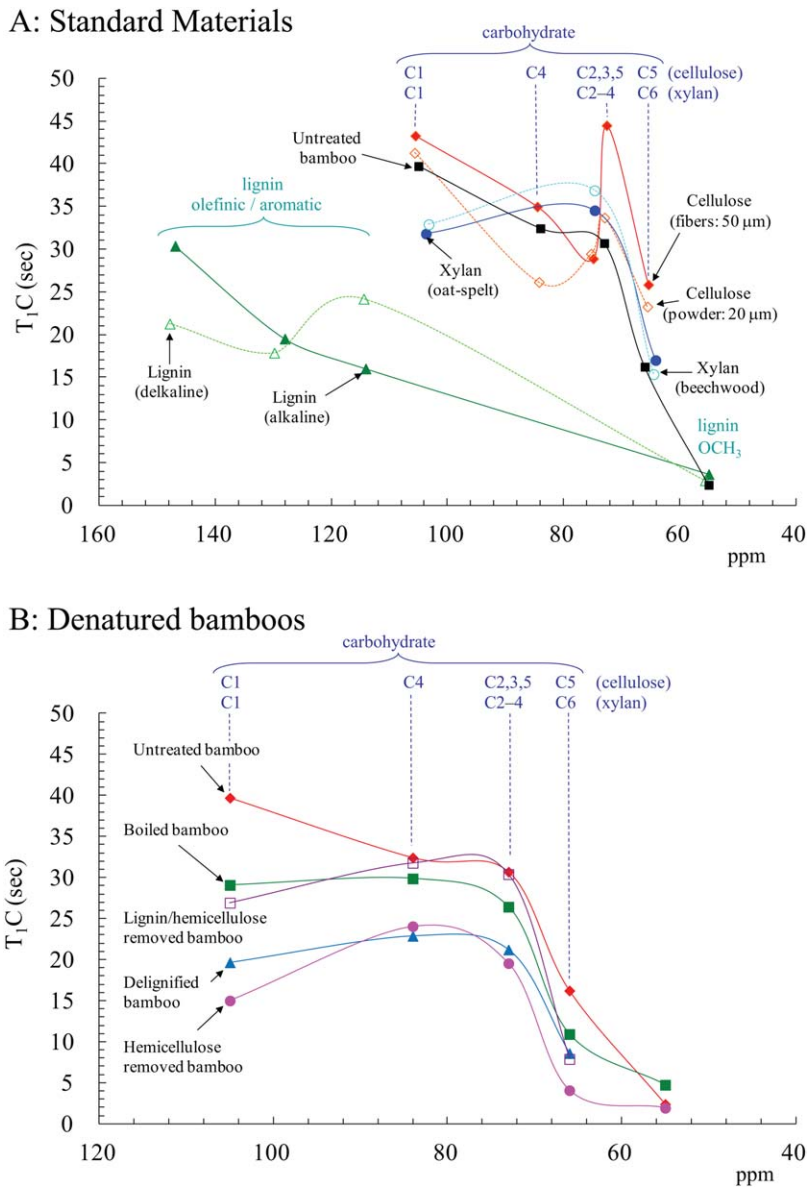

Figure 9. Changes of T_1C values (A: the standard materials; B: denatured bamboos). [Color figure can be viewed in the online issue, which is available at wileyonlinelibrary.com.]

hemicellulose removal process. Similar to ATR-IR spectra [Figure 5(B), line (iii)], the signals of the olefinic and aromatic carbon atoms of lignin were also reduced after the hemicellulose removal process in the ^{13}C DD-MAS NMR spectra [Figure 7(B), line (iv)]. This process occurred via attack on the acetate methyl group first, and then, the hemicellulose unit was decomposed, accompanied by decomposition of the lignin unit. These decompositions brought about the morphological changes in the SEM images [Figures 2(iv′) and 3(iv′)]. The removal of hemicellulose shrank the parenchymal cell; the simultaneous lack of hemicellulose and lignin caused the thin leaf exfoliation from the surfaces of vascular bundles.

Concerning the lignin/hemicellulose removed specimen, for any pulse sequence used to measure ^{13}C MAS NMR spectra [Figure 7, lines (v)], the characteristic signals of lignin (OCH_3, olefinic or aromatic carbon atoms) and hemicellulose (CH_3, C═O) completely disappeared, similar to ATR-IR spectra [Figure 5(B), line (iv)]. The ^{13}C MAS NMR spectra of the lignin/hemicellulose-removed specimen showed almost the same spectra as cellulose powder (20 μm). The relaxation times T_1H and T_1C were also lengthened by the lignin/hemicellulose removal process (Figure 8), evidence that the lignin/hemicellulose removed-specimen retained cellulose polymers came from the T_1H values, which reached similar levels to those of cellulose powder. Losing lignin and hemicellulose caused a shrinkage of the cellular tissue and the remaining parenchymal cells distorted easily, so that both stretched and shrunken shapes were observed in the SEM images of the lignin/hemicellulose removed specimen [Figures 2(v′) and 3(v)].

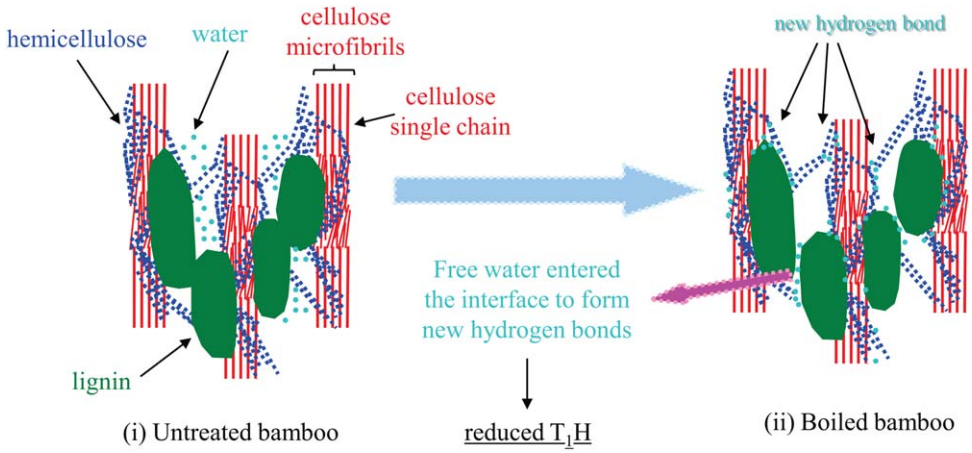

Figure 10. Schematic diagram for cellulose, hemicellulose, and lignin in the nanostructure of bamboo. [Color figure can be viewed in the online issue, which is available at wileyonlinelibrary.com.]

DISCUSSION

This study integrated multiscale information, from the morphology at the microscale to chemical structure and dynamics at the molecular- and nano-scale. The SEM results (section "Morphological analysis of bamboo due to delignification and hemicellulose removal processes") indicated that the parenchymal cells were stretched by the delignification and were shrunk by the hemicellulose removal process. The ATR-IR analysis (section "ATR-IR spectra changes of bamboo due to delignification and hemicellulose removal processes") showed how the characteristic function groups were changed in the vicinity of the surface by the removal of various amounts of lignin and hemicellulose. Solid state NMR (section "Changes in solid state NMR spectra and relaxation time T_1 in the delignification and hemicellulose removal processes") revealed the composition and chemical bonds of each component in the bulk, and changes in molecular dynamics and environment caused by the removal processes. In the case of the nanostructure built by cellulose, hemicellulose, and lignin in woody materials, previous reports have provided various schematic diagrams of its structure.[33–35] Taking those descriptions of the nanostructure into account, we attempted to explain the relationship between the microscale morphology and the chemical structures at the molecular- to nano-scales based on the structure model of cellulose, hemicellulose, and lignin in bamboo shown in Figure 10. Basically, the nanostructure of bamboo is composed of cellulose microfibrils gathered together by single cellulose chains. Hemicellulose bundles the cellulose microfibrils and a three-dimensional network

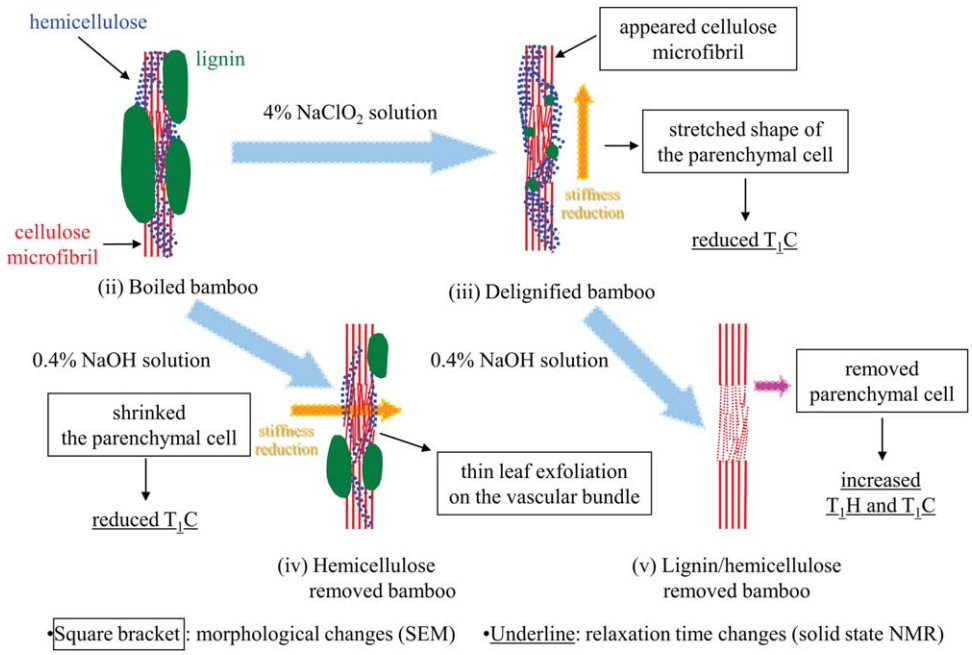

Figure 11. Relationship between the morphology and relaxation times with delignification and hemicellulose removal processes. [Color figure can be viewed in the online issue, which is available at wileyonlinelibrary.com.]

of lignin connects further the outside portions of the hemicellulose. Each cellulose microfibril is bridged by hemicellulose and lignin [Figure 10(i)]. In the boiling process, such a nanostructure built by carbohydrates and lignin does not change but new hydrogen bonds, revealed by the reduction in T_1H values, were formed at the interface of the nanostructure [Figure 10(ii)]. However, the ^{13}C CP-MAS NMR and ATR-IR spectra scarcely changed, except for the new hydrogen bonding, because the inside of the nanostructure was stable against boiling.

In contrast, both delignification and hemicellulose removal processes significantly changed the nanostructure built by carbohydrates and lignin. The changes taking place in the nanostructure of each cellulose microfibril unit containing hemicellulose and lignin are summarized in Figure 11; the relationships between morphological and relaxation time changes are also described. The delignification process removes most of the lignin from the cellulose microfibril while causing little damage to the hemicellulose chain. The removal of lignin was considered to be involved in the observed morphology changes, such as the stretched shape of parenchymal cell [Figure 2(iii′)], due to a reduction of the stiffness in the longitudinal direction of the microfibril [Figure 11(iii)]. On the other hand, the hemicellulose removal process removed lignin as well as hemicellulose, thereby shrinking the parenchymal cell [Figure 2(iv′)] due to a decreasing stiffness in the transverse direction of the microfibril [Figure 11(iv)]. These reductions of stiffness were caused by increasing flexibility of the cellulose microfibril, which also shortened the T_1C values. Furthermore, the delignified specimen more easily released hemicellulose than the boiled specimen because the three-dimensional structure of lignin protected hemicellulose against the NaOH solution. The lignin/hemicellulose-removed specimen had lower stiffness in both the transverse and cross-section directions [Figure 2(v′)], which resulted in the parenchymal cell breaking up into small pieces [Figure 3(v)]. Relaxation via the hydrogen bonding of the more hydrophobic cellulose elongated the T_1H and T_1C values of lignin/hemicellulose-removed specimen [Figure 11(v)].

Considering these results, we would argue that the knowledge obtained by these multiscale instrumental analyses about bamboo specimens is very helpful for the understanding the modification of bamboo and in the development of production processes for bamboo composites. In order to extend the application of our multiscale instrumental analyses, we are now planning analysis of other modified bamboos that are useful as industrial raw materials.

SUMMARY

Several processes to extract bamboo constituents were investigated by multiscale instrumental analyses. SEM images showed that spherical particles were removed from the parenchymal cells of bamboo by boiling and a reduction of the T_1H values indicated that free water formed new hydrogen bonds with carbohydrates and lignin. During the delignification process, SEM images showed stretched parenchymal cells made by the disruption of the three-dimensional lignin network, an event that also influenced the ATR-IR and ^{13}C MAS NMR spectra and lead to decreased T_1C values. SEM images taken during the hemicellulose removal process showed a compression of parenchymal cells in the transverse direction of the microfibril due to removal of hemicellulose, accompanied by a loss of lignin, which was monitored by ATR-IR, ^{13}C MAS NMR, and T_1 analyses. In a combined lignin/hemicellulose removal process, complete removal of hemicellulose and lignin were observed by spectroscopic methods that correlated with the parenchymal cell breaking into pieces which retained vascular bundles in the SEM images. These changes of vascular bundles and parenchymal cells could be explained by a nanostructural model in which cellulose covered by hemicellulose was further connected on the exterior by lignin, whereas lignin in the outermost shell could be extracted on its own, removal of hemicellulose in the middle shell was accompanied by lignin loss.

REFERENCES

1. Ashori, A. *Bioresour. Technol.* **2008**, *99*, 4661.
2. Kalia, S.; Kaith, B. S.; Kaur, I. *Polym. Eng. Sci.* **2009**, *49*, 1253.
3. Yang, Z.; Xu, S.; Ma, X.; Wang, S. *Wood Sci. Technol.* **2008**, *42*, 621.
4. Sun, Y.; Li, L. *J. Agric. Food Chem.* **2010**, *58*, 2253.
5. Li, M.-F.; Fan, Y.-M.; Xu, F.; Sun, R.-C. *J. Appl. Polym. Sci.* **2011**, *121*, 176.
6. Abe, K.; Yano, H. *Cellulose* **2010**, *17*, 271.
7. Vena, P. F.; Görgens, J. F.; Rypstra, T. *Cellul. Chem. Technol.* **2010**, *44*, 153.
8. Li, M.-F.; Fan, Y.-M.; Sun, R.-C.; Xu, F. *Bioresources* **2010**, *5*, 1762.
9. Visakh, P. M.; Thomas, S.; Oksman, K.; Mathew, A. P. *J. Appl. Polym. Sci.* **2012**, *124*, 1614.
10. Yang, F.-C.; Wu, K.-H.; Lin, W.-P.; Hu, M.-K. *Micropor. Mesopor. Mater.* **2009**, *118*, 467.
11. Tokoro, R.; Vu, D. M.; Okubo, K.; Tanaka, T.; Fujii, T.; Fujiura, T. *J. Mater. Sci.* **2008**, *43*, 775.
12. Shi, Q. F.; Mou, H. Y.; Li, Y.; Wang, J. K.; Guo, W. H. *J. Appl. Polym. Sci.* **2012**, *123*, 2828.
13. Hung, K.-C.; Wu, J.-H. *J. Wood Sci.* **2010**, *56*, 216.
14. Yu, X.-C.; Sun, D.-L.; Sun, D.-B.; Xu, Z.-H.; Li, X.-S. *Wood Sci. Technol.* **2012**, *46*, 23.
15. Maunu, S. L. *Prog. Nucl. Magn. Reson. Spectrosc.* **2002**, *40*, 151.
16. Bertocchi, F.; Paci, M. *J. Agric. Food Chem.* **2008**, *56*, 9317.
17. Fujii, Y.; Azuma, J.-I.; Marchessault, R. H.; Morin, F. G.; Aibara, S.; Okamura, K. *Holzforschung* **1993**, *47*, 109.
18. Fujii, Y.; Azuma, J.-I.; Okamura, K. *Horzforschung* **1996**, *50*, 525.
19. Li, M.-F.; Fan, Y.-M.; Xu, F.; Sun, R.-C.; Zhang, X.-L. *Ind. Crop Prod.* **2010**, *32*, 551.
20. He, J.; Cui, S.; Wang, S.-Y. *J. Appl. Polym. Sci.* **2008**, *107*, 1029.
21. He, J.; Tang, Y.; Wang, S.-Y. *Iran. Polym. J.* **2007**, *16*, 807.

22. Nakajima, M.; Kojiro, K.; Sugimoto, H.; Miki, T.; Kanayama, K. *Energy* **2011**, *36*, 2049.
23. Nishida, M.; Nishimura, Y.; Tanaka, T.; Oonishi, M.; Kanematsu, W. *J. Appl. Polym. Sci.* **2012**, *123*, 1865.
24. Nishida, M.; Tanaka, T.; Yamaguchi, T.; Suzuki, K.; Kanematsu, W. *J. Appl. Polym. Sci.* **2012**, *125*, E681.
25. Wang, Y.; Minato, K.; Iida, I. *Mokuzai Gakkaishi* **2006**, *52*, 168.
26. Fung, B. M.; Khitrin, A. K.; Ermolaev, K. *J. Magn. Reson.* **2000**, *142*, 97.
27. Metz, G.; Wu, X. L.; Smith, S. O. *J. Magn. Reson. Ser A* **1994**, *110*, 219.
28. Torchia, D. A. *J. Magn. Reson.* **1978**, *30*, 613.
29. Schwanninger, M.; Rodrigues, J. C.; Pereira, H.; Hinterstoisser, B. *Vib. Spectrosc.* **2004**, *36*, 23.
30. Proniewicz, L. M.; Paluszkiewicz, C.; Wesełucha-Birczyńska, A.; Barański, A.; Dutka, D. *J. Mol. Struct.* **2002**, *614*, 345.
31. Beramendi-Orosco, L. E.; Castro-Díaz, M.; Snape, C. E.; Vane, C. H.; Large, D. J. *Org. Geochem.* **2004**, *35*, 61.
32. Waclaw, K.; Frye, J. S.; Maclel, G. E. *Anal. Chem.* **1982**, *54*, 1419.
33. Alonso, D. M.; Wettstein, S. G.; Dumesic, J. A. *Chem. Soc. Rev.* **2012**, *41*, 8075.
34. Doherty, W. O. S.; Mousavioun, P.; Fellows, C. M. *Ind. Crop Prod.* **2011**, *33*, 259.
35. Vanholme, R.; Van Acker, R.; Boerjan, W. *Trends Biotechnol.* **2010**, *28*, 543.